Geospatial Assessment of Recovery Rates Following a Tornado Disaster

Melissa A. Wagner, Soe W. Myint, and Randall. S. Cerveny

Abstract—Remote sensing has proven to be instrumental in monitoring land alterations from natural disasters and anthropogenic processes. Additionally, geospatial analyses of tornado disasters have provided damage assessments, whereas hazard research has limited recovery evaluation to economic and migration perspectives. This study examines recovery from the 1999 Moore, OK, tornado disaster across three consecutive years, utilizing medium-resolution imagery and a series of image-processing algorithms. Spectral enhancements including normalized difference vegetation index, soil-adjusted vegetation index, urban index (UI), and two new indices, i.e., ShortWave Radiation Index (SWIRI) and Coupled Vegetative Urban Index (CVUI), were utilized in conjunction with a recovery index and statistical thresholds to assess recovery. Classification accuracy assessments prove that geospatial techniques and medium-resolution imagery can capture the rate of recovery with the most effective results noted with SWIRI using the 1.5 standard deviation threshold. Computed annual and Fujita Scale recovery rates indicate that 1) the most severely damaged areas associated with an F5 rating were the slowest to recover whereas the lesser damaged areas (F1–F3) were the quickest to rebuild and 2) complete recovery was never attained, even three years after the event, regardless of the F-scale damage zones. Recovery appears to be a significant and direct function of the level of damage sustained. With these results, decision makers and other policyholders could implement more resilient approaches in reconstructing the more severely damaged areas.

Index Terms—Damage assessment, disaster, reconstruction, recovery, tornado.

I. INTRODUCTION

HAZARD studies have recognized remote-sensing technology as a powerful tool in damage assessment and recovery analyses. These methods have been extensively utilized in monitoring land alterations from natural and anthropogenic processes [1] with ubiquitous satellite coverage, regular data collection, and repeatable independent analyses [2], [3]. Through the manipulation of multispectral data, damaged areas can be detected by correlating alterations in the spectral signatures of ground features with the disaster [2], [4], [5]. Depending on method selection and type of imagery regarding spatial and spectral resolution, varying levels of damage can be discerned, thereby serving as a cost-effective alternative to ground-intensive surveys and aerial photography [2], [3], [5], [6]. Although finer resolution imagery can detail large-scale damages and features [2], drawbacks exist with smaller

coverage, more intensive algorithms, and increasing processing times [7]. Medium-resolution imagery such as Landsat Thematic Mapper (TM) and Landsat Enhanced TM (ETM+) could prove to be more effective in capturing the extent and chaotic nature of damaged areas than finer resolution imagery with its top-view assessment and the development of an effective series of image-processing algorithms.

To analyze disaster impacts and recovery, change detection methods [8] are commonly employed by utilizing spectral enhancements including normalized difference vegetation index (NDVI), multitemporal differencing, and classification techniques. In a severe storm assessment, Bentley *et al.* [4] utilized NDVI differencing derived from Landsat TM imagery to distinguish between hail and wind damage signatures based on significantly lower values associated with plant destruction from hail. Wilkinson and Crosby [9] categorized NDVI-differenced values generated from Landsat TM imagery into light, moderate, and severe damage classes of the April 23–24, 2010 Yazoo, MS, tornado. Yuan *et al.* [2] demonstrated that NDVI differencing produced from Indian Remote Sensing Satellite Linear Imaging Self-Scanning imagery could delineate between F-scale damages using overlay analysis of F-scale damage data in the 1999 Moore, OK, tornado. However, they noted issues in detecting portions of the track along riverbanks due to signature confusion [2]. Jedlovec *et al.* [5] also had some problems with NDVI imagery generated from ASTER and MODIS scenes due to complications of springtime greenness and exogenous land changes [2]–[5] in detecting the 2002 La Plata, MD, tornado path, as well as coarser MODIS imagery.

Other impact studies used different spectral enhancements and geospatial techniques as a means to capture tornado tracks. Myint *et al.* [3] found principal component bands 3 and 4 from Landsat TM imagery to be most effective in discerning the 1999 Moore, OK, tornado path due to contrasting vegetation and soil signatures contrary to Yuan *et al.* [2] findings. They were able to successfully classify the track using these bands and the object-oriented approach, whereas supervised and unsupervised techniques proved to be problematic due to the heterogeneity nature of the urban environment. More recently, Myint *et al.* [6] geospatially categorized F-scale damages within the track using the same imagery with different statistical approaches and window sizes. They noted moderate success with the Getis Index approach and 21×21 window size, suggesting better results with finer resolution imagery.

Regarding tornado damage assessments, land cover types, damage severity, and image quality should be considered with spectral enhancement selection. The ability to detect tornado damage depends on the type of land cover and damage severity

[2], [3], [5]. Urban areas comprising high-class variability and complex spatial arrangements often obscure the track as a result of a similar chaotic pattern [2], [3] with the damage path. Whereas homogeneous regions such as forested areas are easier to discern overall, some vegetative covers are more problematic due to texture, land cover type, and damage magnitude [2], [3], [5]. Damage detection may also be reduced due to image quality, depending on atmospheric absorption and scattering of water vapor and aerosols [2], [5], as well as timing of data collection and storm event. With the complexities of damage detection in rural and urban areas, urban indices or a combination of vegetative and urban indices could better evaluate tornado damage in recovery analyses.

Geospatial techniques have been employed in a variety of postdisaster analyses from wildfires, hurricanes, or tsunamis (e.g., Splinter *et al.* [10], Rodgers *et al.* [11], Barnes *et al.* [12], Reif *et al.* [13], and Mitri and Gitas [14]), focusing on vegetative and urban recovery. Lin *et al.* [15] and Chou *et al.* [16] uncovered spatial disparities in vegetative recovery rates one and six years after the landslide, respectively, using a recovery index and NDVI images (produced from SPOT imagery). Modifying the recovery index, Roemer *et al.* [17] added an impact threshold to define the damaged and recovered regions three years after the 2004 Tsunami using NDVI imagery (derived from IKONOS scenes). Validated from ground-truth data, their analysis proved effective in discerning recovery with overall accuracies of 80.77%. This method could be useful in distinguishing damaged and recovered regions after the disaster by taking into account the minor deviations in index values that can occur annually. Unlike the aforementioned analyses, Reif *et al.* [13] employed hyperspectral imagery, decision-based classification, and LIDAR data, noting volume increases (decreases) in bare soil and low vegetation (structures and medium and tall vegetation) three years after Hurricane Katrina. Focusing solely on urban recovery, Ward *et al.* [18] found recovery disparities using a Geographic Information Systems (GIS)-based spatial recovery index three years after Hurricane Katrina, loosely connecting recovery and social vulnerability. Burton *et al.* [19] also discovered recovery variations from Hurricane Katrina using repeat photography, GIS methodologies, and spatial statistics correlating the biophysical impact with recovery.

One aspect, however, that has only recently become researched is postdisaster recovery utilizing remote-sensing methodologies (e.g., Splinter *et al.* [10], Rodgers *et al.* [11], Barnes *et al.* [12], Reif *et al.* [13], and Mitri and Gitas [14]). While these and other studies have shown that evaluation of postdisaster recovery is possible, only non-geospatial assessments focusing on migration and economic perspectives have been utilized in examining recovery rates from tornado disasters. Cross [20] and Paul [21] found recovery in terms of migration responses to be a function of the amount of aid received and economic opportunities obtained. DeSilva *et al.* [22] inferred recovery based on property values rebounding to pretornado prices with the 1999 Moore, OK, tornado using county assessor's data. Analyzing a small segment of the track, they discovered that housing prices in the more severely damaged areas lagged in market value before rebounding three years

later, illustrating the effect that the biophysical impact has on recovery rates [19], [22]–[26].

Most disaster research utilizing remote sensing has focused on small-scale disasters, such as hurricanes, tsunamis, earthquakes, and floods. Few studies have examined tornado events, limiting their scope to damage assessments. Depending on intercepted infrastructure and damage magnitude, the magnitude of damage can actually be greater than large-scale events, creating lasting effects on the landscape. Therefore, the need to examine not only the initial impact but also recovery using geospatial means still exists. Examining recovery objectively can provide valuable information regarding restoration disparities from the biophysical impact and lead to better decision-making policies in the recovery process.

Consequently, this study addresses the following questions: 1) How effective are geospatial techniques in assessing recovery using medium-resolution imagery? 2) Are recovery rates uniform with regard to damage class (e.g., Fujita scale)? These questions are investigated by employing remote-sensing and GIS technologies to examine recovery from the 1999 Moore, OK, tornado using Landsat TM and Landsat ETM+ imagery. Utilizing spectrally enhanced imagery, a recovery index, and statistical thresholds, damaged and recovered regions were classified and spatially analyzed with F-scale contour data produced from ground surveys [2], [27]. In this analysis, we define recovery as the restoration of the landscape in both rural and urban regions, i.e., returning back to the original state as measured by predisaster indexed values. Annual and F-scale recovery rates were computed to investigate the role that the biophysical impact plays in recovery. Decision makers could use this information to implement more resilient strategies in the most severely damaged areas.

II. STUDY AREA AND DATA DESCRIPTION

A. Study Area

This study examines the recovery from the 1999 Moore, OK, tornado spawned from the May 3, 1999, supercell outbreak. This tornado is considered as one of the deadliest tornado disasters, having the strongest measurable winds ever recorded [28]. Labeled A9 in Fig. 1, this tornado touched down at the central portion of Grady County and traveled 38 mi before dissipating on the eastern side of Oklahoma City in Oklahoma County. Within its path, the cities of Moore and Bridge Creek sustained the most damage based on dense infrastructure and inferred intensity rating of an F5 on the Fujita Scale [27]. Following National Oceanic and Atmospheric Administration's publication "Storm Data" [29], our research only examines the continuous track labeled A9. Additionally, the damage assessment of the Moore tornado was concluded prior to the introduction of the Enhanced Fujita Scale [30].

This particular tornado serves as a good example for analyzing the recovery process because of its track length, path, varying degrees of damages, and detailed damage information. This tornado tracked 38 mi on the ground, traversing different land cover types in both rural and urban areas. Consequently, damage magnitudes varied significantly with
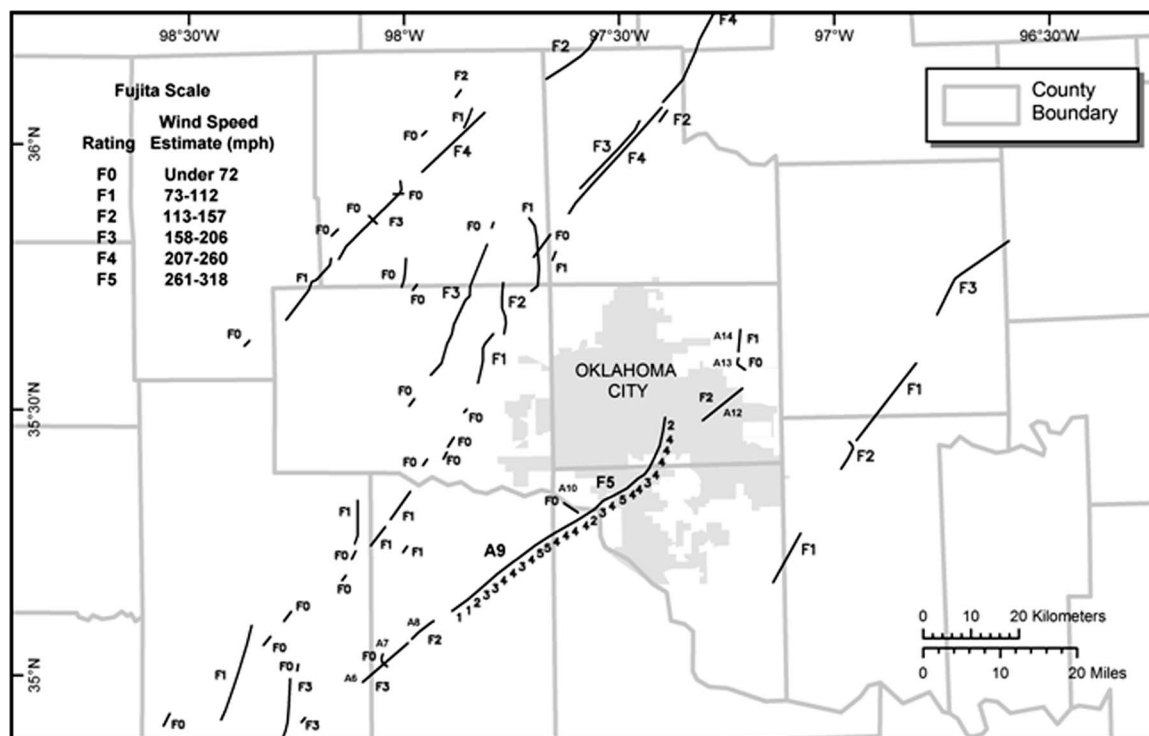
Fig. 1. Map of the recorded tornado locations and associated F-scale ratings during the May 3, 1999, Tornado Outbreak in Central Oklahoma. http://www.srh.noaa.gov/images/oun/wxevents/19990503/maps/bigoutbreak.gif.

Fujita Scale ratings, ranging from minor damages correlated with an F1 to incredible damages associated with an F5 [31]. Additionally, this tornado was the only track that could be clearly identified in satellite imagery with highly detailed F-scale information provided by the most knowledgeable experts [27]. With such a diverse cross-section of factors involved, this tornado disaster provides an opportune case study to monitor recovery.

B. Data and Data Preprocessing

For this multitemporal study, both Landsat TM and Landsat ETM+ imagery at 30-m spatial resolution were utilized, with seven multispectral channels spanning from blue to thermal portions of the electromagnetic spectrum. All of the multispectral bands were utilized, except for the thermal and panchromatic bands due to coarse resolution and Landsat ETM+ availability, respectively. Cloud-free imagery for Central Oklahoma (path 28, row 35) were obtained prior to the tornado disaster on June 26, 1998, and after the disaster on May 12, 1999, May 30, 2000, April 23, 2001, and September 17, 2002. Ideally, imagery should be collected within two weeks of the anniversary date [8], [32]; for each scene, however, cloud contamination proved to be problematic. Therefore, scenes for 1998 and 2002 were selected based on similar vegetative greenness [33] to ensure successful change detection. Images after 2002 were not collected due to the lack of cloud-free scenes prior to another tornado event within the study area on May 8, 2003.

The selected scenes were preprocessed to reliably monitor recovery [34]. Relative radiometric corrections were performed to minimize distortion of actual surface reflectance from haze [33], [35] and convert digital numbers into apparent reflectance using the Cos(t) model in IDRISI Taiga (Version 16). These images were imported into ERDAS Imagine 9.3 and coregistered to reduce pixel misregistration [6] below the standard root-mean-square error of 0.5 pixels. To minimize reflectance variations between scenes [32], [33], [36], post-tornado imagery was normalized based on densely vegetative values in the pre-tornado image. Each image was layer stacked and subset to extract the tornado-affected region covering 1689.62 km^2 (upper left longitude 97° 44′ 36.537″ W and latitude 35° 35′ 32.057″ N and lower right longitude 97° 19′ 4.331″ W and latitude 35° 12′ 0.343″ N).

In conjunction with Landsat imagery, F-scale contours [2], [27] developed from the Oklahoma Weather Center were utilized to define the damage track (see Fig. 2). Using a high-resolution F-scale map provided by Speheger *et al.* [27], F-scale contours were digitized and georeferenced in Universal Transverse Mercator Projection Zone 14 with World Geodetic System 1984 spheroid using the U.S. Geological Survey Quadrangles, i.e., Oklahoma City North and Oklahoma City South, at a scale of 1:100 000. The track was clipped to the post-tornado image to exclude a small portion extending into the adjacent scene below. This decision to omit less than 10 mi of the track in a densely vegetative region was based on the requirement of different radiometric corrections tailored to each scene. This would have more than likely complicated results by introducing errors; therefore, this scene and segment of track was not included in the analysis. The F-scale contour data were transformed into an area-of-interest file (AOI) to extract recovery information for all F-scale zones.

Fig. 2.   Superimposed F-scale contour data, with the outermost contour F1 rating increasing in damage scale intensity to the innermost F5 rating contour overlaid on the zoomed-in section of the study area displayed in grayscale.

III. Methods

A. Spectral Indices

To evaluate recovery, spectral enhancements were generated in the form of vegetative, urban, and a combination of these two indices. NDVI and soil-adjusted vegetation index (SAVI) were used to assess vegetative health [17], [37], [38] and distinguish between damaged and reconstructed areas based on known index values (see Table I). Urban index (UI) images [39] were also produced to better discern recovery in residential areas and other built environments due to its wider range between vegetative and man-made surfaces [40] (see Table I). By understanding the range of values associated with vegetative health and land cover types, land cover changes associated with the tornado could be monitored through changing index values [2], [3]. Therefore, NDVI, SAVI, and UI images were generated for 1998, 1999, 2000, 2001, and 2002.

For this study, we created two new indices to better evaluate recovery. The first index merged UI and NDVI into what we call the Coupled Vegetative Urban Index (CVUI). The aim of this index is to successfully capture damaged regions in both vegetative and urban land covers based on their sensitivity to the spectral responses of these materials (see Table I). The second new index, which is named ShortWave Infrared Index (SWIRI), also contains a vegetative assessment component using the near-infrared band and first midinfrared band (see Table I). The inclusion of the first midinfrared band in this index could help indicate the state of surface features (damaged and recovered), as this band is commonly used to delineate moisture content in vegetation and soils [41]. As a result, both SWIRI and CVUI could prove to be more effective than the aforementioned indices. Hence, SWIRI and CVUI outputs were produced for

1998, 1999, 2000, 2001, and 2002 with an example of the 1999 SWIRI image shown in Fig. 3.

Using the indexed images (NDVI, SAVI, UI, SWIRI, and CVUI), recovery was evaluated for the years of 2000, 2001, and 2002, utilizing a recovery equation. This equation was modified from Roemer *et al.* [17]

$$R = \left[\frac{\text{Index}_2 - \text{Index}_1 + 2}{\text{Index}_1 - \text{Index}_0 + 2} \right] \qquad (1)$$

where R is recovery; and Index_2, Index_1, and Index_0 are the images for the recovery year, post-tornado year, and pre-tornado year, respectively (see Fig. 4). The differenced images were rescaled using a factor of two to overcome a computer algorithm problem of near-zero values in the denominator. This also ensured the inclusion of minor to moderately damaged areas that could have otherwise been excluded with a threshold. The resulting images were then divided accordingly for each index and year assessed.

B. Recovery Analysis

Recovery was determined by employing different statistical thresholds from the aforementioned images to account for minor annual deviations. While recovered regions should obtain a value of 1.0, annual differences due to atmospheric and climate conditions could still potentially affect index values despite data corrections. Therefore, three possible outcomes were generated based on common thresholds of 0.5, 1.0, and 1.5 standard deviations from the mean of the entire recovery scene listed in Table II. Values that fell within the selected standard deviation were classified as recovered, whereas out-of-bound pixels were regarded as still damaged. To capture only recovered pixels in the subsequent year(s), a mask was applied to 2001 and 2002 recovery images, following the aforementioned procedures. This process was repeated for each index (NDVI, SAVI, UI, SWIRI, and CVUI), yielding a total 45 possible recovery outcomes. To extract recovery information only for the tornado-affected region, we used track AOI to subset these images.

To compare recovery outcomes, accuracy assessments were performed and analyzed for each scene. As suggested by Congalton [42], the minimum 50 points per class (recovered and still damaged) were collected using a stratified random sampling approach [42], [43], generating a total of 100 points per scene. These results generated error matrices listing overall, producer's, and user's accuracies, which express the values of categorized points relative to the verified ground truth category [42], [43]. This is a very effective way of representing accuracy in that both errors of inclusion and omission are presented [42]. More specifically, producer's accuracy is the probability of a pixel being correctly identified, and user's accuracy is the total number of correct pixels in a category divided by the total number of classified pixels for that category [42]. These accuracies were averaged according to index and threshold and ranked to determine the best results. Error uncertainty with the recovery index was assessed using the best results to calculate a combined standard error from a random sampling of 100 points per recovery scene collected outside the tornado track.

TABLE I
LIST OF INDEX, EQUATION, AND UTILITY

Index	Equation	Utility
NDVI	$\dfrac{\text{NIR (Band 4) - Red (Band 3)}}{\text{NIR (Band 4) + Red (Band 3)}}$	Monitors vegetative health and distinguishes between vegetative biomass (higher positive values for healthy vegetation), man-made surfaces, bare soils and barren surface, water, clouds, snow and ice (near zero to negative values)
SAVI	$(1 + L) * \dfrac{\text{NIR (Band 4) - Red (Band 3)}}{\text{NIR (Band 4) + Red (Band 3) + L}}$	Vegetative index similar to NDVI except introduces a soil correction factor L that minimizes external effects from solar illumination variations due to atmospheric conditions or soil reflective properties
UI	$\dfrac{\text{NIR (Band 7) - Red (Band 4)}}{\text{NIR (Band 7) + Red (Band 4)}}$	Discriminates between man-made surfaces and vegetative cover with high positive values assigned to artificial surfaces and low negative values assigned to vegetation
SWIRI	$\dfrac{\text{NIR (Band 5) - Red (Band 4)}}{\text{NIR (Band 5) + Red (Band 4)}}$	Assigns low negative values to vegetation and high positive values to urban surfaces with the added benefit of moisture detection and discriminating between different man-made and geological surfaces
CVUI	$\dfrac{\text{(MIR (Band 7) - Red (Band 4))*(NIR (Band 4) - Red (Band 3))}}{\text{(MIR (Band 7) + Red (Band 4))*(NIR (Band 4) + Red (Band 3))}}$	Combines NDVI and UI to assess vegetative health and distinguish between urban surfaces assigning low positive values to vegetation and artificial surfaces assigned high positive values

Fig. 3. Post-tornado SWIRI image of the Moore, OK, tornado-impacted region with tornado path outlined in white.

Using the best results, annual recovery rates were calculated from the following equation:

$$\text{Recovery} = \left[\frac{\text{Recovery area}}{\text{Total Area}} \right] * 100. \qquad (2)$$

To illustrate annual recovery changes, a composite map displaying damaged and recovered regions was produced. F-scale recovery rates were calculated using the aforementioned equation by overlaying F-scale contour data onto each annual map.

IV. RESULTS

Before quantitatively evaluating recovery, we analyzed the behavior of the two new indices SWIRI and CVUI. Sampled index values of various land cover types listed in Table III reveal that both SWIRI and CVUI exhibit similar values to UI, producing low positive values for bare soil and low negative values for healthy vegetation. Both SWIRI and CVUI show positive (negative) correlations with UI (SAVI and NDVI) curves but deviate slightly with CVUI values falling in between lower UI values and higher SWIRI values.

Accuracy assessments of the aforementioned indices and thresholds revealed trends according to threshold and index type. The 0.5 standard deviation threshold performed poorly among all the indices, with the least effective results of 65.0% produced by SAVI based on the averaged results in Table IV. Both vegetation indices underperformed with their best accuracies of 75.7% and 76.3%, which are still short of the 80% land use classification [45]. UI consistently outperformed the vegetative indices with the 1.0 standard deviation accurately classifying 80% of the damaged and recovered regions, followed by 79.7% with the 1.5 standard deviation threshold. The new indices SWIRI and CVUI proved to be most effective at capturing recovery with overall accuracies of 80.3% and 81.7% for 1.0 and 1.5 standard deviation thresholds, respectively.

Upon further inspection, damaged areas proved to be more difficult to classify with lower producer's and user's accuracies. Although producer's accuracies remained at 80.0% or above, these accuracies were, on average, 19.0% lower than recovered pixels, indicating more problems excluding recovered pixels from the damaged class. The user's accuracies deviated more than the producer's, with accuracies ranging from 41.3% with SAVI using the 0.5 standard deviation threshold to 73.3% with SWIRI using 1.5 standard deviation threshold. This illustrated more difficulty in correctly identifying still damaged areas largely in part from exogenous land use changes such as agricultural practices and newly built environments. While some
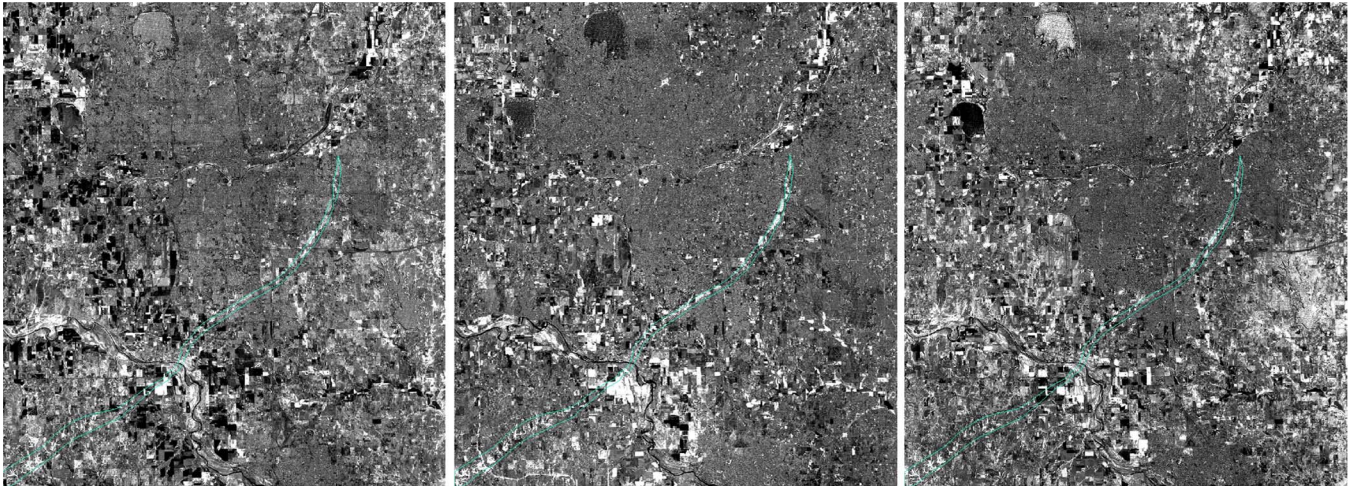
Fig. 4. SWIRI recovery images of the Moore, OK, tornado-impacted region with tornado path outlined in white for (a) 2000, (b) 2001, and (c) 2002.

TABLE II
LIST OF RECOVERED RANGES CORRESPONDING TO 0.5, 1.0, AND 1.5
STANDARD DEVIATION THRESHOLDS FOR EACH INDEX AND YEAR

Index	Year	Mean	0.5		1		1.5	
			Min	Max	Min	Max	Min	Max
NDVI	2000	1.015	0.987	1.044	0.958	1.072	0.930	1.101
	2001	1.022	0.977	1.068	0.931	1.113	0.886	1.159
	2002	1.000	0.968	1.033	0.935	1.065	0.903	1.098
SAVI	2000	1.009	0.991	1.028	0.972	1.046	0.954	1.065
	2001	1.016	0.986	1.046	0.956	1.076	0.926	1.106
	2002	1.006	0.984	1.028	0.962	1.050	0.940	1.072
UI	2000	0.985	0.951	1.019	0.917	1.053	0.883	1.087
	2001	1.007	0.961	1.054	0.914	1.100	0.868	1.147
	2002	0.996	0.958	1.034	0.920	1.072	0.882	1.110
SWIRI	2000	0.985	0.961	1.009	0.937	1.033	0.913	1.057
	2001	1.010	0.973	1.047	0.936	1.084	0.899	1.121
	2002	1.028	1.000	1.057	0.971	1.085	0.943	1.114
CVUI	2000	0.989	0.965	1.013	0.941	1.037	0.917	1.061
	2001	1.002	0.966	1.039	0.929	1.075	0.893	1.112
	2002	1.005	0.978	1.033	0.950	1.060	0.923	1.088

of these regions were still visible as distinct linear shapes in McClain County (see Fig. 5), this problem was best handled using SWIRI, with the largest threshold followed by CVUI. Error analysis using the best results validated the effectiveness of the recovery index with a combined standard error of 0.049 for the SWIRI recovery scenes.

Using the best results (SWIRI at 1.5 standard deviation), derived F-scale recovery rates (Table V) revealed two significant findings in this analysis. The first major finding is the consistent theme that the incredibly damaged regions were the slowest to recover, whereas minor to moderately damaged areas reported the highest recovery rates. More specifically, recovery in F5 damage zones consistently lagged behind F0/F1 zones by a noticeable difference of 18.9%, 17.2%, and 18.7% in 2000, 2001, and 2002, respectively. This trend shown in Fig. 6 was also evident in F4 damaged zones as the most substantial impacted areas (F4–F5) only recovered by an average of 66.6% during the first year, compared with 79.3% recovery in the

F0/F1–F3 regions. Even by the third year after the tornado event (2002), recovery for the F4–F5 zone was only 84.0%, whereas F0/F1–F3 damages had recovered to 95.7%. This observation led to the second important finding that complete recovery was never attained in any F-scale damage zones.

Annual differences and trends in recovery rates became more apparent when plotting F-scale recovery rate information (Fig. 6). Most recovery occurred within the first two years after the event with relatively minor changes between 2001 and 2002. The 2000–2001 rates displayed a 12.0%–16.2% increase in recovery, whereas the 2001–2002 recovery rates increased from 1.1% to 4.2%. The F5 recovery rate nearly stabilized with only a 1.1% increase in 2002 with a total of 75.3% recovered. Interestingly, recovery lines were not parallel across all damage levels, indicating differences in the degree of recovery as a function of F-scale damage. However, some similarities could be seen between F0/F1–F3 recovery rates with nearly identical slopes and a relatively narrow range in the three years assessed.

V. DISCUSSION

As previously detailed, we analyzed recovery rates for three years following the 1999 Moore, OK, tornado utilizing medium-resolution imagery and found three important findings. The first finding was that medium-resolution satellite imagery such as Landsat TM and ETM+ can be used to establish recovery rates by providing a top-view assessment. The two new indices SWIRI and CVUI developed for disaster management and recovery proved to be best suited for recovery assessments over UI, NDVI, and SAVI as a result of band combinations. In addition to index types, recovery was most effectively captured using the 1.5 standard deviation threshold, with the best overall results noted with SWIRI. The larger range of recovery values was more reflective of actual recovery similar to previous studies [15], [17], which employed thresholds to analyze recovery.

Regardless of threshold selection, damaged pixels proved to be the most difficult to accurately classify due to land use changes. In particular, agricultural changes (fallow versus active fields) were repeatedly misidentified as damaged when performing classification accuracy assessments. Additionally,

TABLE III
SAMPLED MEANS OF DIFFERENT LAND COVER CLASSES

Index	Residential	Commercial	Bare Soil	Fallow Agriculture	Active Agriculture	Dense Vegetation	Water
NDVI	0.462	0.108	0.147	0.202	0.721	0.849	-0.295
SAVI	0.297	0.072	0.121	0.150	0.509	0.502	-0.089
UI	-0.315	0.027	0.067	0.063	-0.492	-0.662	-0.177
SWIRI	-0.148	0.061	0.070	0.132	-0.237	-0.360	-0.128
CVUI	-0.156	-0.003	0.007	0.009	-0.366	-0.567	0.053

TABLE IV
AVERAGED ACCURACY ASSESSMENTS LISTED BY INDEX AND STANDARD DEVIATION THRESHOLD. (Overall = Overall accuracy, Prod. = Producer's accuracy, User's = User's Accuracy, R = Rank, PR = Producer's Rank, UR = User's Rank)

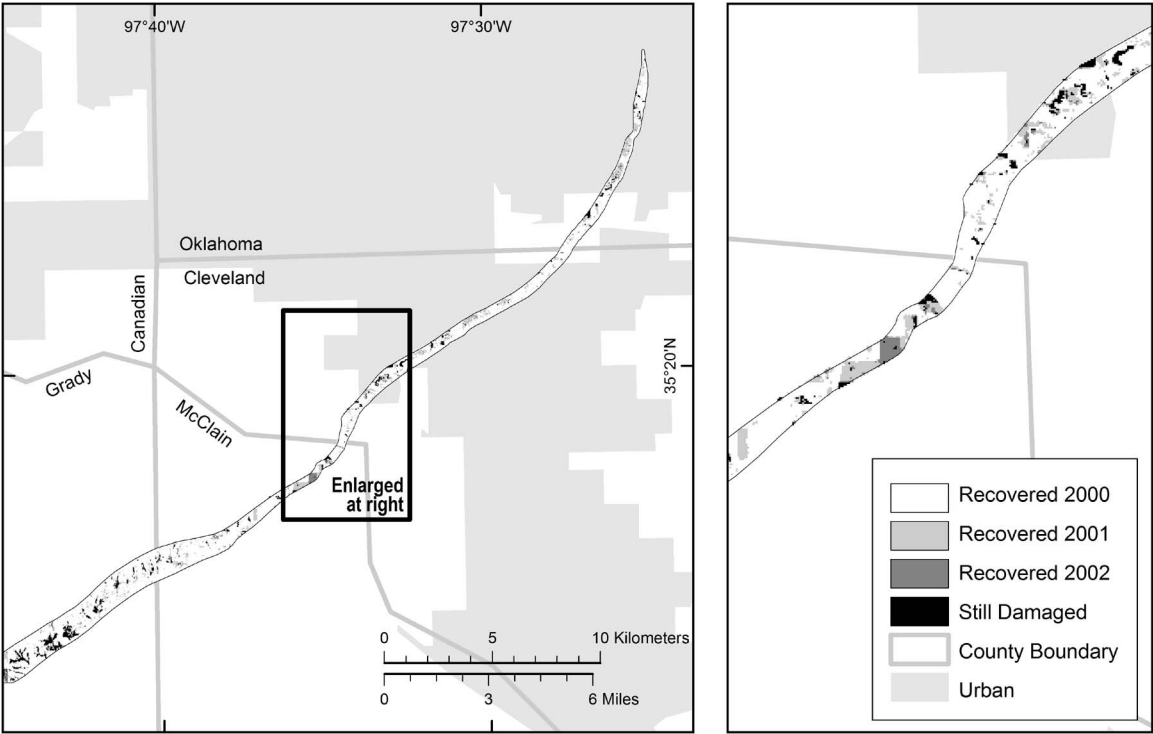| Index	St Dev	Overall		Recovery				Damaged			
		Overall	R	Prod.	User's	PR.	UR	Prod.	User's	PR.	UR
SAVI	0.5	65.0%	15	62.0%	94.0%	15	4	86.7%	41.3%	14	15
SAVI	1.0	75.7%	8	67.3%	93.3%	9	8	89.1%	54.0%	7	10
SAVI	1.5	74.3%	9	67.7%	93.3%	8	8	89.1%	55.3%	8	9
NDVI	0.5	68.7%	14	62.6%	93.3%	14	8	88.2%	44.0%	11	14
NDVI	1.0	76.3%	7	69.5%	94.0%	7	4	90.8%	58.7%	2	7
NDVI	1.5	71.0%	12	66.2%	86.0%	12	15	80.0%	56.0%	15	8
UI	0.5	73.0%	11	66.4%	93.3%	11	8	89.6%	52.7%	6	12
UI	1.0	80.0%	5	74.6%	91.3%	3	12	88.9%	68.7%	9	4
UI	1.5	79.0%	6	72.9%	94.0%	6	4	91.4%	64.7%	1	6
SWIRI	0.5	73.7%	10	66.9%	94.0%	10	4	90.3%	53.3%	4	11
SWIRI	1.0	80.3%	3	74.3%	92.7%	5	10	90.6%	68.0%	3	5
SWIRI	1.5	81.7%	1	77.1%	90.0%	2	14	88.2%	73.3%	12	1
CVUI	0.5	70.3%	13	64.1%	92.7%	13	10	86.8%	48.0%	13	13
CVUI	1.0	80.3%	3	74.5%	92.0%	4	11	89.9%	68.7%	5	3
CVUI	1.5	81.7%	1	77.3%	90.7%	1	13	88.7%	72.7%	10	2

Fig. 5. Recovered and damaged regions for 2000, 2001, and 2002 using SWIRI and 1.5 standard deviation threshold. (a) Track overview. (b) Inset.

TABLE V
RECOVERY RATES FOR F-SCALE ZONES USING SWIR INDEX
WITH 1.5 STANDARD DEVIATION THRESHOLD

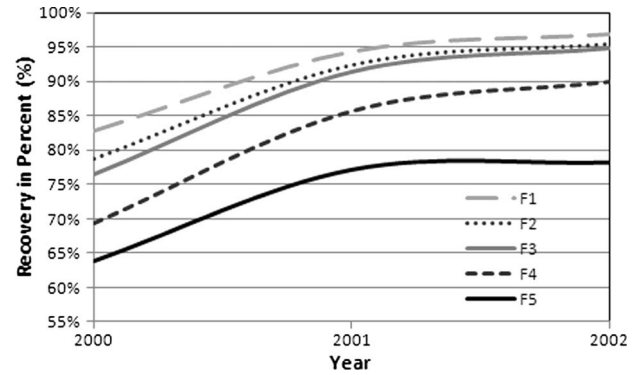| Year	Fscale Zone	Recovered Area (km)	Damaged Area (km)	Total Area (km)	Recovery Rate
2000	1	8149.5	1701.0	9850.5	82.7%
	2	6468.3	1744.2	8212.5	78.8%
	3	6130.8	1881.0	8011.8	76.5%
	4	3174.3	1400.4	4574.7	69.4%
	5	439.2	249.3	688.5	63.8%
2001	1	9293.4	557.1	9850.5	94.3%
	2	7591.5	621.0	8212.5	92.4%
	3	7322.4	689.4	8011.8	91.4%
	4	3916.8	657.9	4574.7	85.6%
	5	531.0	157.5	688.5	77.1%
2002	1	9544.5	306.0	9850.5	96.9%
	2	7842.6	369.9	8212.5	95.5%
	3	7596.0	415.8	8011.8	94.8%
	4	4110.3	464.4	4574.7	89.8%
	5	538.2	150.3	688.5	78.2%

Fig. 6. Graph for the 1999 Moore, OK, tornado-impacted region displaying F-scale recovery rates in percent for 2000, 2001, and 2002 as established by the recovery index.

new construction was more likely to be misclassified as damaged, especially if this transformation occurred in previously healthy vegetation areas. Such a change occurred with the construction of the H.E. Bailey Turnpike Norma Spur (OK 4) in the lower left quadrant of all 2000 recovery images (Fig. 5). This land use change was repeatedly misidentified as damaged among all the thresholds during the classification accuracy assessments and may have also affected the surrounding vegetation. Consequently, these exogenous changes did affect the overall accuracy of the recovery index but were rather minimal in comparison to the amount of recovery that was accurately identified.

The second and most critical finding is that the incredibly damaged areas associated with an F5 rating were the slowest to rebuild, whereas the lesser-damaged regions with F0/F1 ratings reported the highest recovery rates. These results were consistent throughout 2000, 2001, and 2002 as recovery in F5 damaged areas lagged behind F0/F1 damaged zones by a considerable difference of 18.9%, 17.2%, and 18.7%, respectively. Lower recovery rates for F4 damaged areas also illustrated the profound effect that the biophysical impact has on recovery. This finding is conclusive with other hazard studies [19], [22]–[26] that have also linked recovery rates to the biophysical impact.

Higher recovery in the F0/F1–F3 damaged areas could be explained by contrasting differences between these regions and F4 and F5 zones. Maximum damage indicators for F0/F1–F3 ratings are noted by missing roofs and, in some cases, removal of walls, whereas well-constructed houses are completely leveled in F4 zones with even more catastrophic damage in F5 regions [31]. As a result, recovery in lesser damaged areas (F0/F1–F3) would typically require less financial resources to draw upon and time to complete the repairs, thereby explaining similar and faster recovery rates [19], [46]. Unlike lesser damaged areas,

recovery in the most severely damaged areas (F4 and F5) would require more financial resources, decision-making policies regarding construction, and, consequently, more time to rebuild with the possibility of relocating to another site [19], [26], [46].

In addition to anthropogenic recovery, vegetation regeneration is a function of the damage magnitude and plant size [47]–[49]. Generally, minor-wind damages to vegetation will reorient or blow over the plant, resulting in only minor disruptions in photosynthetic activity [4]. Therefore, much of the vegetation survives and recovers quickly back to the pre-tornado state [4]. Contrary to this, intense winds are more likely to snap vegetation destroying it; thus, recovery is much slower [47], [48]. Additionally, the speed of vegetation regeneration depends on plant size before the disaster, as smaller plants tend to recover quicker than large trees [13], [47]–[49]. Typically, larger vegetation will take several years, if not decades, for complete restoration based on tree size [47]. This aspect explains not only vegetative response with recovery rates but also the location of still damaged areas in the bottom portion of the track (see Fig. 5) due to the densely forested region.

The third important finding was that, even by 2002 (three years after the tornado event), complete recovery was never achieved in any F-scale damaged zones. By 2002, the least damaged regions (F0/F1) had rebuilt to 96.9%, whereas recovery in the most incredibly damaged areas (F5) had reached only 78.2%. This could be partially attributed to a relatively, short time frame, given that a subsequent F4 tornado hit the same study area on May 8, 2003. As a result, any continued recovery from the May 3, 1999, tornado disaster could not be analyzed. Additionally, decision-making policies and political institutions could have also affected recovery in urban areas, with different land use changes set aside to mitigate future events or help improve current economic status. For example, after the 2007 Greensburg, Kansas, tornado, city officials decided to rebuild the town using green initiatives and rezoned a few residential areas into commercial in hopes of attracting economic opportunities [50]. Individual decisions to relocate could have also impacted recovery based on damage severity, financial resources including disaster relief, and psychological decisions as seen with Hurricanes Katrina and Rita [51]. With regards to vegetation regeneration, large vegetation will take several years, if not decades, to return to pre-tornado conditions, thus contributing to incomplete recovery [47].

In addition to the biophysical aspect of disaster, preexisting conditions could also affect recovery in terms of social vulnerabilities and place-based vulnerabilities. Social vulnerabilities due to lower socioeconomic status, lack of resources, and poor housing quality can magnify the impact of the disaster and consequently affect the ability to fully recover [52]–[56]. Such examples of this can be seen in the more recent cases of the 2004 Tsunami, Hurricane Katrina, and the 2010 Haitian Earthquake [56], [57]. These factors could have contributed to the incomplete recovery after the tornado disaster but were not analyzed in this analysis.

Certain geographic locations may also be physically and socially susceptible to a given hazard, creating place-based vulnerabilities [55], [58]. These regions can have higher degrees of vulnerability based on the clustering of social and biophysical characteristics within the hazard zone [58]. The city of Moore, OK, was previously struck by an F2 tornado in October 1998, but that tornado produced considerably smaller damages with a path length of only 2 mi. Nonetheless, this could have affected individual and commercial decisions in terms of rebuilding or relocating. One known example occurred in a residential section of Moore, OK, as decision makers chose not to rebuild in this section due to the past occurrence of tornadoes in this area and instead dedicated the land as a city park. Other place-based vulnerabilities, similar to those previously mentioned, could have also existed within the track and affected individual and policy-making decisions on recovery, given the short time between disasters.

VI. CONCLUSION

With regards to remote-sensing capabilities, this research sets forth the direction of recovery analysis for tornado disasters using cost-effective resolution imagery such as Landsat TM and ETM+, in conjunction with geospatial techniques. This type of analysis provides a top-view assessment that could aid decision-making processes in urban planning and developers in the recovery process. Within this research, the two indices SWIRI and CVUI that were developed for disaster management and recovery analysis should also be explored with the traditionally employed indices (NDVI, SAVI, and UI) to better capture both the initial impact and the recovery process.

With regard to tornado disaster recovery, we have identified that the incredibly damaged areas associated with an F5 rating were the slowest to rebuild, whereas the lesser damaged regions with F0/F1 ratings reported the highest recovery rates. Even by 2002, three years after the 1999 Moore, OK, tornado, complete recovery was never achieved in any F-scale damaged zones. Such findings stress the importance that the scope and magnitude of the disaster has on the recovery process. Decision makers and other policyholders could better understand the importance of the biophysical impact and implement more resilient approaches to recovery within the most severely damaged areas.

ACKNOWLEDGMENT

REFERENCES

[1] M. D. Mura, J. A. Benediktsson, F. Bovolo, and L. Bruzzone, "An unsupervised technique based on morphological filters for change detection in very high resolution images," *IEEE Geosci. Remote Sens. Lett.*, vol. 5, no. 3, pp. 433–437, Jul. 2008.

[2] M. Yuan, M. Dickens-Micozzi, and M. A. Magsig, "Analysis of tornado damage tracks from the 3 May tornado outbreak using multispectral satellite imagery," *Weather Forecast.*, vol. 17, no. 3, pp. 382–398, 2002.

[3] S. Myint, M. Yuan, R. Cerveny, and C. Giri, "Comparison of remote sensing image processing techniques to identify tornado damage areas from Landsat TM data," *Sensors*, vol. 8, no. 2, pp. 1128–1156, Feb. 2008.

[4] M. L. Bentley, T. L. Mote, and P. Thebepanya, "Using Landsat to identify thunderstorm damage in agricultural regions," *Bull. Amer. Meteorol. Soc.*, vol. 83, no. 3, pp. 363–376, Mar. 2002.

[5] G. J. Jedlovec, U. Nair, and S. L. Haines, "Detection of storm damage tracks with EOS data," *Weather Forecast.*, vol. 21, no. 3, pp. 249–267, Jun. 2006.

[6] S. Myint, M. Yuan, R. Cerveny, and C. Giri, "Comparison of remote sensing image processing techniques to identify tornado damage areas from Landsat TM data," *Sensors*, vol. 8, pp. 1128–1156, 2008.

[7] E. A. Wentz, W. L. Stefanov, M. Netzband, M. Moller, and A. J. Brazel, *Global Mapping of Human Settlements: Experiences, Datasets, and Prospects.* Boca Raton, FL: CRC Press, 2009, pp. 191–204.

[8] A. Singh, "Digital change detection techniques using remotely sensed data," *Int. J. Remote Sens.*, vol. 10, pp. 989–1003, 1989.

[9] D. W. Wilkinson and M. K. Crosby, "Rapid assessment of forest damage from tornadoes in Mississippi," *Photogramm. Eng. Remote Sens.*, vol. 76, no. 12, pp. 1298–1301, 2010.

[10] K. D. Splinter, D. R. Strauss, and R. B. Thomlinson, "Assessment of post-storm recovery of beaches using video imaging techniques: A case study at Gold Coast Australia," *IEEE Trans. Geosci. Remote Sens.*, vol. 49, no. 12, pp. 4704–4716, Dec. 2011.

[11] J. C. Rodgers, III, A. W. Murrah, and W. H. Cooke, "The impact of Hurricane Katrina on the coastal vegetation of the Weeks Bay Reserve, Alabama from NDVI data," *Estuaries Coasts*, vol. 32, no. 3, pp. 496–507, 2009.

[12] C. F. Barnes, H. Fritz, and J. Yoo, "Hurricane disaster assessments with image-driven data mining in high resolution satellite imagery," *IEEE Trans. Geosci. Remote Sens.*, vol. 45, no. 6, pp. 1631–1640, Jun. 2007.

[13] M. K. Reif, C. L. Macon, and J. M. Wozencraft, "Post-Katrina Land-cover, elevation and volume change assessment along the south shore of Lake Pontchartrain, Louisiana, U.S.A," *J. Coastal Res.*, no. 62, pp. 30–39, Spring 2011.

[14] G. H. Mitri and I. Z. Gitas, "Mapping post-fire vegetation recovery using EO-1 Hyperion imagery," *IEEE Trans. Geosci. Remote Sens.*, vol. 48, no. 3, pp. 1613–1618, Mar. 2010.

[15] C. Y. Lin, H. M. Lo, W. C. Chou, and W. T. Lin, "Vegetation recovery assessment at the Jou-Jou Mountain landslide area caused by the 921 earthquake in central Taiwan," *Ecol. Model.*, vol. 176, no. 1/2, pp. 75–81, Aug. 2004.

[16] W. C. Chou, W. T. Lin, and C. Lin, "Vegetation recovery patterns assessment of landslides caused by catastrophic earthquake: A case study in Central Taiwan," *Environ. Monitoring Assessment*, vol. 152, no. 1–4, pp. 245–257, May 2009.

[17] H. Römer, J. Jeewarongkakull, G. Kaiser, R. Ludwig, and H. Sterr, "Monitoring post-tsunami vegetation recovery in Phang-Nga province, Thailand—A remote sensing based approach," *Int. J. Remote Sens.*, vol. 33, no. 10, pp. 3090–3121, 2012.

[18] S. M. Ward, M. Leitner, and J. Pine, "Investigating recovery patterns in post disaster urban settings: Utilizing geospatial technology to understand post-Katrina recovery in New Orleans, Louisiana," *Geospatial Tech. Urban Hazard Disaster Anal.*, vol. 2, pp. 355–372, 2010.

[19] C. Burton, J. T. Mitchell, and S. L. Cutter, "Evaluating post-Katrina recovery in Mississippi using repeat photography," *Disasters*, vol. 35, no. 3, pp. 488–509, Jul. 2011.

[20] J. Cross, "Megacities and small towns: Different perspectives on hazard vulnerability," *Environ. Hazards*, vol. 3, no. 2, pp. 63–80, Jun. 2001.

[21] B. Paul, "Evidence against disaster-induced migration: The 2004 tornado in north-central Bangladesh," *Disasters*, vol. 29, no. 4, pp. 370–385, Dec. 2005.

[22] D. G. De Silva, J. B. Kruse, and Y. Wang, "Catastrophe-induced destruction and reconstruction," *Nat. Hazards Rev.*, vol. 7, no. 1, pp. 19–25, Feb. 2006.

[23] D. Dacy and H. Kunreuther, *The Economics of Natural Disasters: Implication for Federal Policy*. New York: Free Press, 1969.

[24] P. Hass, K. Eugene, and W. Robert, *Reconstruction Following Disaster*, M. J. Bowden, Ed. Cambridge, MA: MIT Press, 1977.

[25] E. Yasui, "Community vulnerability and capacity in post-disaster recovery: The cases of Mano and Mikura neighborhoods in the wake of the 1995 Kobe earthquake," Ph.D. dissertation, Dept. Geography, Univ. British Columbia, Vancouver, BC, Canada, 2007.

[26] D. P. Aldridge, "The power of people: Social capital's role in recovery from the Kobe earthquake," *Nat. Hazards*, vol. 56, no. 3, pp. 595–611, 2010.

[27] D. A. Speheger, C. A. Doswell, III, and G. J. Stumpf, "The tornadoes of 3 May 1999: Event verification in Central Oklahoma and related issues," *Weather Forecast.*, vol. 17, no. 3, pp. 362–381, Jun. 2002.

[28] R. S. Cerveny, J. Lawrimore, R. Edwards, and C. Landsea, "Extreme weather records: Compilation, adjudication and publication," *Bull. Amer. Meteorol. Soc.*, vol. 88, no. 6, pp. 853–860, Jun. 2007.

[29] National Climate Data Center, 2010. [Online]. Available: http://www4.ncdc.noaa.gov/cgiwin/wwcgi.dll?wwEvent~Storms

[30] J. R. McDonald, "Development of an enhanced Fujita scale for estimating tornado intensity," in *Proc. 21st Conf. Severe Local Storms, Amer. Meteorol. Soc.*, Boston, MA, 2002, pp. 174–177.

[31] T. T. Fujita, "Experimental classification of tornadoes in FPP scale," Univ. Chicago, Chicago, IL, SMRP Res. Rep. 98, 1971.

[32] J. R. Jensen, K. Rutchey, M. S. Koch, and S. Narumalani, "Wetland change detection in the everglades water conservation area 2A using a time series of normalized remotely sensed data," *Photogramm. Eng. Remote Sens.*, vol. 61, no. 2, pp. 199–209, 1995.

[33] A. S. Mahiny and B. Turner, "A comparison of four common atmospheric correction methods," *Photogramm. Eng. Remote Sens.*, vol. 73, no. 4, pp. 361–368, Apr. 2007.

[34] J. R. G. Townshend, C. O. Justice, C. Gurney, and J. McManus, "The impact of pixel misregistration on change detection," *IEEE Trans. Geosci. Remote Sens.*, vol. 30, no. 5, pp. 1054–1060, Sep. 1992.

[35] P. S. Chavez, "An improved dark-object subtraction technique for atmospheric scattering correction of multispectral data," *Remote Sens. Environ.*, vol. 24, no. 3, pp. 459–479, Apr. 1988.

[36] F. G. Hall, D. E. Strebel, J. E. Nickeson, and S. J. Goetz, "Radiometric rectification: Towards a common radiometric response among multidate, multisensor images," *Remote Sens. Environ.*, vol. 35, no. 1, pp. 11–27, Jan. 1991.

[37] J. W. Rouse, R. H. Haas, J. A. Schell, and D. W. Deering, "Monitoring vegetation systems in the Great Plains with ERTS," in *Proc. 3rd Earth Resour. Technol. Satellite-1 Symp. Tech. Presentations, Section A1*, S. C. Freden, E. P. Mercanti, and M. Becker, Eds., 1973, pp. 309–317.

[38] A. R. Huete, "A soil-adjusted vegetation index (SAVI)," *Remote Sens. Environ.*, vol. 25, no. 3, pp. 295–309, Aug. 1988.

[39] M. Kawamura, S. Jayamamana, and Y. Tsujiko, Comparison of urbanization and environmental condition in Asian cities using satellite remote sensing data1997. [Online]. Available: http://www.a-a-r-s.org/acrs/proceeding/ACRS1997/Papers/PS197-8.htm

[40] P. Villa, "Imperviousness indexes performance evaluation for mapping urban areas using remote sensing data," in *Proc. Joint Urban Remote Sens. Event*, Paris, France, 2007, pp. 1–6.

[41] F. F. Sabins, *Remote Sensing—Principles and Interpretation*, 3rd ed. New York: W.H. Freeman, 1997, p. 494.

[42] R. G. Congalton, "A review of assessing the accuracy of classifications of remotely sensed data," *Remote Sens. Environ.*, vol. 37, no. 1, pp. 35–46, Jul. 1991.

[43] S. W. Myint, C. P. Giri, L. Wang, Z. Zhu, and S. Gillette, "Identifying mangrove species and their surrounding land use and land cover classes using an object oriented approach with a lacunarity spatial measure," *GIScience Remote Sens.*, vol. 45, no. 2, pp. 188–208, 2008.

[44] R. G. Congalton and K. Green, *Assessing the Accuracy of Remotely Sensed Data: Principles and Practice*. Boca Raton, FL: Lewis Publ., 1999, p. 137.

[45] R. M. Hord and W. Brooner, "Land-use map accuracy criteria," *Photogramm. Eng. Remote Sens.*, vol. 42, no. 5, pp. 671–677, May 1976.

[46] J. R. Stevenson, C. T. Emrich, J. T. Mitchell, and S. L. Cutter, "Using building permits to monitor disaster recovery: A spatio-temporal case study of coastal Mississippi following Hurricane Katrina," *Cartograph. Geograph. Inf. Sci.*, vol. 37, no. 1, pp. 57–68, Jan. 2010.

[47] C. J. Peterson and A. Rebertus, "Tornado damage and initial recovery in three adjacent, lowland temperate forests in Missouri," *J. Vegetation Sci.*, vol. 8, no. 4, pp. 559–564, Sep. 1997.

[48] C. J. Peterson, "Damage and recovery of tree species after two different tornadoes in the same old growth forest: A comparison of infrequent wind disturbances," *Forest Ecol. Manage.*, vol. 135, no. 1–3, pp. 237–252, Sep. 2000.

[49] R. W. Myster and M. P. Malahy, "Tornado effects on damage resprouting and spatial heterogeneity on the Cross Timbers ecotone of Oklahoma," *J. Plant Ecol.*, vol. 3, no. 3, pp. 157–163, 2010.

[50] B. K. Paul and D. Che, "Opportunities and challenges in rebuilding tornado-impacted Greensburg, Kansas as stronger, better, and greener," *Geojournal*, vol. 76, no. 1, pp. 93–108, Feb. 2011.

[51] C. K. Myers, T. Slack, and J. Singlemann, "Social vulnerability and migration in the wake of disaster: The case of Hurricanes Katrina and Rita," *Population Environ.*, vol. 29, no. 6, pp. 271–291, Jul. 2008.

[52] D. Liverman, "Drought impacts in Mexico: Climate, agriculture, technology, and land tenure in Sonora and Puebla," *Ann. Assoc. Amer. Geograph.*, vol. 80, no. 1, pp. 49–72, Mar. 1990.

[53] P. Blaikie, T. Cannon, I. Davis, and B. Wisner, *At Risk: Natural Hazards, People's Vulnerability, and Disasters*. London, U.K.: Routledge, 1994.

[54] S. L. Cutter, "Vulnerability to environmental hazards," *Progr. Human Geography*, vol. 20, no. 4, pp. 529–539, Dec. 1996.

[55] S. Cutter, B. Boruff, and W. L. Shirley, "Social vulnerability to environmental hazards," *Social Sci. Quart.*, vol. 84, no. 2, pp. 242–261, Jun. 2003.

[56] M. Kaplan, F. G. Renaud, and G. Lüchters, "Vulnerability assessment and protective effects of coastal vegetation during the 2004 Tsunami in Sri Lanka," *Nat. Hazards Earth Syst. Sci.*, vol. 9, no. 4, pp. 1479–1494, Aug. 2009.

[57] S. L. Cutter, C. T. Emrich, J. T. Mitchell, B. Boruff, M. Gall, M. Schmidtlein, C. Burton, and G. Melton, "The long road home: Race, class, and recovery from Hurricane Katrina," *Environ. Sci. Policy Sustain. Develop.*, vol. 48, no. 2, pp. 8–20, Mar. 2006.

[58] S. L. Cutter, *American Hazardscapes: The Regionalization of Hazards and Disasters*. Washington, DC: Joseph Henry Press, 2000.

Melissa A. Wagner was born in Inglewood, CA. She received the B.S. degree in geography from Wright State University, Dayton, OH, in 1999 and the M.A. degree in geography, in 2011, from Arizona State University, Tempe, where she currently working toward the Ph.D. degree in tornado disaster recoveries and damage assessments.

Soe W. Myint received the B.Sc. degree from Rangoon University, Yangon, Myanmar, the Postgraduate Diploma from the International Institute for Aerospace Survey and Earth Sciences, Enschede, the Netherlands, the M.Sc. degree from the Asian Institute of Technology, Pathum Thani, Thailand, and the Ph.D. degree from Louisiana State University, Baton Rouge.

He is Associate Professor of geographical sciences with Arizona State University, Tempe.

Dr. Myint has served as the President, the Vice President, the Regional Director, and the Membership Chair of the American Society for Photogrammetry and Remote Sensing-Southwest U.S. Region and is currently serving as the Chair of the Remote Sensing Specialty Group, Association of American Geographers.

Randall S. Cerveny received the B.S., M.A., and Ph.D. degrees from the University of Nebraska, Lincoln.

He is currently a President's Professor of Geographical Sciences with Arizona State University, Tempe, concentrating on climate change and climate extremes.